Medicinal Chemistry Research (2019) 28:1923–1938
https://doi.org/10.1007/s00044-019-02424-3

MEDICINAL CHEMISTRY RESEARCH

ORIGINAL RESEARCH

Macrocyclic effect on inhibitory activity: a modeling study on MerTK inhibitors

Swapnil P. Bhujbal[1] · Seketoulie Keretsu[1] · Pavithra K. Balasubramanian[1] · Seung Joo Cho[1,2]

Received: 4 June 2019 / Accepted: 13 August 2019 / Published online: 31 August 2019

Abstract

Macrocyclic ring structures could have drug-like properties such as membrane permeability, metabolic stability, binding affinity, selectivity, and high-biological activities. Synthesized macrocyclic inhibitors have been studied and the effect of ring size has gained attention from drug design community. Marsault et al. showed a positive correlation between ring size and inhibitory activity against rennin. On the other hand, De Clercq et al. suggested that there would be some optimum ring size for histone deacetylase inhibitory activity. Therefore, macrocyclic effects appear elusive while intriguing. In this study, we have selected a large set of macrocyclic inhibitors (14–20-membered rings) to study macrocyclic effect on MerTK using molecular modeling techniques. We carefully positioned all the cyclic inhibitors into the binding pocket utilizing available information obtained from both experimental and theoretical means. Then, from the resultant binding poses, the ligand–receptor interactions were analyzed. Unlike previous reports, we could not observe any relevance between ring size and inhibitory activity. However, there is a correlation between the number of hydrogen bonds and inhibitory activity. Among these hydrogen-bonding interactions, active site residues Arg727, and Asn728 as well as two signature interactions at the hinge region were found to be crucial for MerTK inhibition. Furthermore, the importance of number of hydrogen bonding was further validated statistically by means of 3D-QSAR techniques such as CoMFA and CoMSIA. The involvement of Arg727 and Asn728 was checked graphically by CoMSIA hydrogen-bonding donor map. This outcome could be helpful for more potent MerTK inhibitor design. In addition, more detailed studies on ring size effect would be desirable to understand macrocyclic effects.

Keywords MerTK · Antagonists · Molecular docking · 3D-QSAR · CoMFA · CoMSIA

Introduction

Naturally occurring macrocyclic compounds have the ring sizes that span from 11- to 16-membered rings, most frequently 14 membered (Madsen and Clausen 2011). Macrocyclic ring structures have been reported to show a favorable impact on essential properties required for drugs such as membrane permeability (Giordanetto and Kihlberg 2013), metabolic stability, increased binding affinity and selectivity (Mallinson and Collins 2012), and overall pharmacokinetics (Driggers et al. 2008; Gradillas and Perez-Castells 2010). They are reported to display remarkably high biological activities and have equilibrium between flexibility and conformational preorganization to achieve optimal binding properties with respect to their biological targets (Marsault and Peterson 2011, 2017; Wessjohann et al. 2005). Some of the naturally occurring macrocyclic compounds are erythromycin (antibiotic), epothilone B (anticancer), tacrolimus (immunosuppressant), and bryostatins (protein kinase C inhibitor) (Bridger et al. 1995; Marsault and Peterson 2011, 2017; Wessjohann et al. 2005).

Artificial inhibitors with large ring structures were synthesized and also studied for inhibitory activity against various targets. There have been various studies about ring

Electronic supplementary material The online version of this article (https://doi.org/10.1007/s00044-019-02424-3) contains supplementary material, which is available to authorized users.

✉ Pavithra K. Balasubramanian
pavithrabioinfo@gmail.com

✉ Seung Joo Cho
chosj@chosun.ac.kr

[1] Department of Biomedical Sciences, College of Medicine, Chosun University, Gwangju 501-759, Republic of Korea

[2] Department of Cellular·Molecular Medicine, College of Medicine, Chosun University, Gwangju 501-759, Republic of Korea

size effects over the potency of inhibitors. Marsault and Peterson (2011) reported that macrocyclic inhibitors of renin showed increase in inhibitory activity with increase in ring size (from 10- to 14-membered rings). In contrast, histone deacetylase inhibitors exhibited higher potency with a 14-membered ring over a 16-membered ring. In that study, the potency was lower when the ring size was bigger (Marsault and Peterson 2011). Bridger and co-workers performed structure-activity relationship for phenylenebis (methylene)-linked bistetraazamacrocycles against HIV (HIV-1 and HIV-2 replication) (Bridger et al. 1995). They observed that increasing the ring size from 10 to 14 resulted in higher anti-HIV activity. But, further increase in the ring size resulted in a substantial reduction of the potency (Bridger et al. 1995; Hawkins 2017; Watts et al. 2014). Therefore, the ring size effect is very interesting, but the nature of its interaction has not been well investigated.

Receptor tyrosine kinases (RTKs) are important transmembrane receptors that regulate key signal transduction such as apoptosis, migration, cell proliferation, and invasion of many cancers (Hojjat-Farsangi 2014; Yu et al. 2015a). Mer receptor tyrosine kinase (MerTK) is a member of the TAM family of RTKs, which comprises Tyro3, Axl, and MerTK (Cummings et al. 2013; Knubel et al. 2014). TAM receptors are type I transmembrane glycoproteins, composed of an extracellular domain containing tandem fibronectin type III repeats, tandem immunoglobulin-related domains and a protein kinase c-like intracellular kinase domain (Evans et al. 2017; Graham et al. 1994; Knubel et al. 2014). TAM family members have highly conserved kinase domain (>70% identity), and encompasses a distinct KW(I/L)A(I/L)ES active site that varies from other RTKs (Evans et al. 2017; Lemke and Rothlin 2008; Linger et al. 2008).

Inhibition of MerTK presents unique clinical challenge since drugs that target MerTK would also inhibit the normal proteins in noncancerous cells. There are few compounds that have been reported to exhibit potent antagonism against MerTK such as UNC569 derivatives (Schlegel et al. 2013), ONO-9330547 (Craven et al. 1995; Neubauer et al. 1994), CVO-102, R428, and BMS-777607 (Driggers et al. 2008). UNC569 derivatives and ONO-9330547 increased the sensitivity to chemotherapy and decreased colony formation of acute lymphoblastic leukemia cells and a pediatric tumor cell line (BT12) (Nguyen et al. 2014). CVO-102 has been shown to have remarkable activity in preventing blood clotting and also shows promising anticancer agent in late preclinical development (Holland et al. 2010). R428 and BMS-777607 exhibit activity against Mer but are ~4-fold to 15-fold more selective for Axl (Holland et al. 2010; Holland et al. 2005).

To study MerTK and inhibitor interactions, docking, molecular dynamics (MD) and receptor-based 3D-QSAR (3D-Quantitative Structure-Activity Relationship) studies were reported with various pyrimidine derivatives such as pyrazolo-[3,4-d]-pyrimidines (Hamzah and Tjahjono), pyridine-substituted pyrimidines (Yu et al. 2015b) pyridinepyrimidines (Balupuri et al. 2015), and pyrimidine-based derivatives (Balupuri et al. 2016). Yu et al. (2015b) and Liang et al. (2006) reported that hinge region residues Pro672 and Met674 are very important for MerTK inhibition. These two amino acids have been found important with experimental studies (McIver et al. 2017; Wang et al. 2016). X-ray structures (PDB ID: 5K0X and 5K0K) show that MerTK hinge region residues (Pro672 and Met674) bind to the co-crystallized inhibitors (McIver et al. 2017; Wang et al. 2016). In another study, abovementioned amino acids were also suggested crucial by docking analyses. In addition, 107 MerTK inhibitors were used to generate a ligand-based pharmacophore model. Six compounds with new scaffolds were identified as MerTK inhibitors by virtual screening using this model (Zhou et al. 2016).

In this study, we have selected a series of macrocyclic MerTK inhibitors having various ring sizes (from 14- to 20-membered rings) to study ring size effect and factors affecting MerTK inhibitory activity. To this end, we used various simulation techniques such as docking, MD, and 3D-QSAR methods.

Materials and methods

Overall procedure

Simple alignment schemes such as atom by atom matching could not be applied due to the complex nature of the macrocyclic ring structure. In recent studies, Hawkins (2017) and Watts et al. (2014) reported that sampling of low energy conformers of macrocycles is difficult due to the large ring size and flexibility of these molecules. The existing techniques such as stochastic methods based on Monte Carlo-simulated annealing, distance geometry are not convenient for conformational sampling of macrocyclic molecules (Hawkins 2017; Watts et al. 2014).

MD should be one of the reasonable simulation methods to deal with macrocyclic ring structure (Driggers et al. 2008). So, we have employed MD for pose selection of macrocyclic compounds inside the receptor to provide reliable molecular alignments. Fortunately, there exists information about seemingly important amino acid residues such as Pro672 and Met674 (Balupuri et al. 2015; McIver et al. 2017). Hydrogen-bonding interactions with these two hinge region residues mimic the interaction of ATP with MerTK, which have been considered crucial for the inhibitor recognition.

Using these hydrogen-bonding interactions at the hinge region as the anchoring points, the inhibitors could be placed inside the receptor in a reasonable way. Then the structures were optimized by MD followed by energy minimization and structure sampling. The resultant structures of ligands were used as input structures for subsequent receptor-based 3D-QSAR studies. Comparative molecular field analysis (CoMFA) and comparative molecular similarity indices analysis (CoMSIA) were used to understand the structural requirements of MerTK inhibitors.

Molecular docking

Prior to the docking process, the protein structure was prepared as follows: polar hydrogen was added, Kollman and Gasteiger charges and AD4 atom-types were assigned. Autodock 4.0 (Huey et al. 2007) was used to perform docking. Docking protocol was validated by re-docking of extracted co-crystallized ligand from the crystal structure (PDB code: 5K0K) into the active site of the protein. Active site was defined by the same residues as used in the previous studies (Balupuri et al. 2015, 2016). The most potent compound from the dataset was docked into the active site of MerTK. Active site grid was created using the x, y, and z coordinates of the active site. Dimensions of this grid were extended to $80 \times 80 \times 80$ points with a grid spacing of 0.375 Å. The number of Genetic algorithm (GA) run was set to 100 and docking was executed using the Lamarckian genetic algorithm (LGA). The resultant docked conformations were clustered into groups with default RMS deviations of 0.5 Å.

A docked pose based on the docking score and the two key hydrogen-bonding interactions at the hinge region (Pro672, Met674) was selected as the representative binding pose. Since the dataset comprises macrocyclic compounds with various ring sizes (from 14- to 20-membered rings), we docked all the compounds. Since Autodock does not allow flexibility of macrocyclic ring structures, we have performed MD simulations for structural optimization and relaxation using SYBYL-X 2.1 program.

Structure optimization and sampling

SYBYL-X 2.1 was used for MD to generate conformers of these macrocyclic ring structures. As a first step, a dynamics run for 100 ps was performed using NVT ensemble at 300 K and with a time step of 1 fs. Trajectories were recorded every 5 ps for the MD runs. Boltzmann random velocity was selected as the initial velocity. The rest of the parameters were chosen as default. Tripos force field was used for the minimization of all the compounds. Gasteiger–Marsili charges were applied to the protein-ligand complex. The important residues (Pro672, Met674) forming key hydrogen bond (H-bond) interactions were constrained. From the several conformers generated, one conformation was selected considering two criteria. i.e., energy and the presence of two key H-bond interactions as mentioned above. Final conformers selected for the compounds were used for the 3D-QSAR study.

Test set/training set selection for 3D-QSAR analyses

A series of 68 macrocyclic pyrimidines reported as potent MerTK inhibitors with their biological activities (IC_{50} values) was collected for this study (McIver et al. 2017; Wang et al. 2016). These inhibitors exhibit various ring sizes (from 14- to 20-membered rings). SYBYL-X 2.1 was used to sketch all the 68 structures and optimized by energy minimization with Tripos force field (Clark et al. 1989). Biological data expressed as IC_{50} values were converted into pIC_{50} ($-\log IC_{50}$) values. The pIC_{50} values cover 4.24 log units, which signify the dataset is acceptable for a QSAR study (Wold et al. 1984). The dataset was divided into a training set of **46** compounds for model derivation and a test set of **22** compounds for external predictability. The test sets were selected by considering different macrocyclic ring sizes and biological activity. The compounds were classified into high, medium, and low active ones depending on the biological activities. Subsequently, **22** compounds were randomly taken from the three activity classes and chosen as the test set. Docked conformation of the most active compound was taken as a template to sketch the rest of the compounds in the dataset. All the ligands taken for the docking studies were energy minimized to find the most reasonable poses within the receptor. The chemical structures and biological activity values of all the compounds are depicted in Table 1.

3D-QSAR (CoMFA and CoMSIA)

In CoMFA, correlation of biological properties of compounds with steric and electrostatic potential energies are calculated using Lennard-Jones and Coulombic potentials, respectively (Cramer et al. 1988b). The dataset compounds should be aligned in their bioactive conformations to develop a reasonable model (Kamath and Buolamwini 2003). The dataset compounds were aligned using a common substructure-based alignment method with template molecule (most active compound **6**). The choice of appropriate partial charge scheme is important to obtain robust 3D-QSAR models. Previous studies reported the necessity of considering more appropriate atomic charges rather than default CoMFA charges (Gadhe et al. 2012; Madhavan et al. 2012). We derived 3D-QSAR models using different charge calculation schemes to study the

Table 1 Structure and biological activity values of macrocyclic pyrimidines as MerTK inhibitors

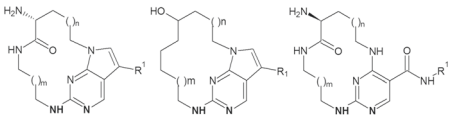

Compound	R^1	m	n	IC_{50} (nm)	pIC_{50} (nm)
1*		2	1	3.9	8.409
2		4	1	17	7.770
3*		6	1	30	7.523
4*		2	2	8.9	8.051
5		4	2	2.2	8.658
6		6	2	0.8	9.097
7*		1	1	4.1	8.387
8		2	1	5.6	8.252
9	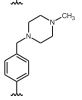	3	1	1.8	8.745
10*		4	1	9.6	8.018
11		1	2	8.0	8.097

influence of these charge schemes on the 3D-QSAR models. The partial atomic charges were applied for each ligand by using different charge schemes i.e., Gasteiger–Hückel, Hückel, Gasteiger–Marsili (Gasteiger and Marsili 1980), Del-Re (Del Re 1958), Pullman (Berthod et al. 1967), MMFF94 (Halgren 1999) and AM1-BCC (Jakalian et al. 2002).

Default parameters were used to generate the CoMFA model. A sp^3 hybridized carbon as probe atom with + 1 charge and a grid spacing of 2.0 Å was used. The partial least squares (PLS) regression was used to develop statistically reasonable 3D-QSAR models. In the PLS analysis, CoMFA descriptors were used as independent variables and biological activity values (pIC_{50}) were used as dependent variables. PLS analysis with leave-one-out cross-validation was executed to evaluate the reliability of the models developed (Cramer 1993; Li et al. 2013). The squared cross-validated correlation coefficient (q^2) value, an optimal number of components (ONC) and standard deviation of prediction (SEP) were calculated using PLS analysis. A column filtering value of 2.0 was used. A noncross-validation analysis was then carried out using the

12	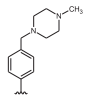	2	2	4.0	8.398
13*	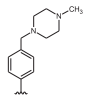	3	2	3.0	8.523
14*	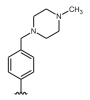	4	2	2.6	8.585
15	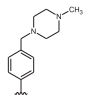	1	3	4.1	8.387
16		2	3	5.0	8.301
17		3	3	3.1	8.509
18		4	3	4.9	8.310
19		3	2	140	6.854
20		3	2	150	6.824
21		3	2	86	7.066
22		3	2	160	6.796
23*		3	2	170	6.770
24	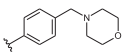	3	2	16	7.796
25	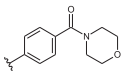	3	2	8.1	8.092
26	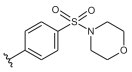	3	2	11	7.959
27	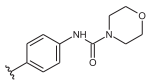	3	2	30	7.523
28	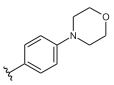	3	2	32	7.495
29*		3	2	54	7.268

obtained ONC by cross-validation to calculate the squared correlation coefficient (r^2), F-test value (F) and standard error of estimate.

In CoMSIA (Klebe et al. 1994), steric, electrostatic, hydrophobic, H-bond donor, and H-bond acceptor descriptors were considered. All five CoMSIA similarity indices were calculated using a probe atom of radius 1.0 Å. An attenuation factor of 0.30 was used. The CoMSIA models were calculated between the grid point and each atom of the molecule by a Gaussian function (Klebe et al. 1994). The CoMSIA models with different combinations were generated with the same lattice box used as in CoMFA

30*		3	2	13	7.886
31		3	2	80	7.097
32		3	2	94	7.027
33		2	1	61	7.215
34		1	1	200	6.699
35*		3	1	760	6.119
36		4	1	230	6.638
37		5	1	91	7.041
38*		6	1	62	7.208
39		1	2	3200	5.495
40		2	2	140	6.854
41*		3	2	36	7.444
42		4	2	4.4	8.357
43*		5	2	4.1	8.387
44*		6	2	6.2	8.208
45	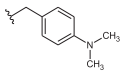	4	2	6.4	8.194
46*	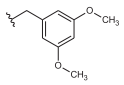	4	2	25	7.602
47	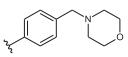	4	2	6.0	8.222
48	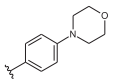	4	2	9.5	8.022
49*	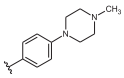	4	2	4.3	8.367
50		4	2	6.3	8.201
51*		4	2	4.4	8.357
52		4	2	22	7.658
53	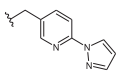	4	2	1.5	8.824

calculations. Among the possible combinations, a model with reasonable statistical values in terms of q^2 and r^2 was selected as the final CoMSIA model. 3D-QSAR results were interpreted graphically by the field contribution maps. The developed models were checked for predictive ability and robustness using various validation techniques, which includes bootstrapping, progressive scrambling, an external test set validation, rm^2 metric calculations and concordance correlation coefficient (CCC) (Chirico and Gramatica 2012). Bootstrapping for 100 runs and the progressive scrambling of 100 runs with 2–10 bins were performed to validate the model's predictability (Gadhe et al. 2012). The models were also validated by the predictive correlation coefficient (r^2_{pred}).

54*		4	2	6.5	8.187
55		4	2	14	7.854
56	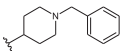	4	2	2.9	8.538
57*	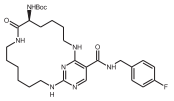	-	-	54	7.268
58	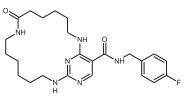	-	-	59	7.229
59	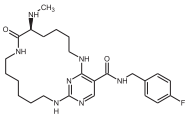	-	-	11	7.959
60	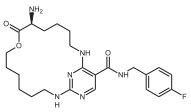	-	-	3.9	8.409
61*	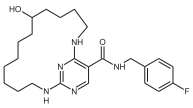	-	-	68	7.168
62	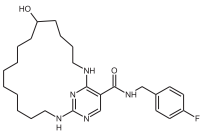	-	-	140	6.854
63*	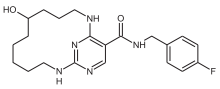	-	-	21	7.678
64	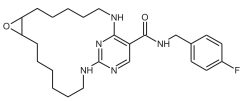	-	-	480	6.319
65	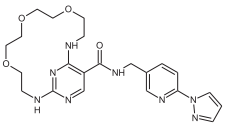	-	-	770	6.114
66	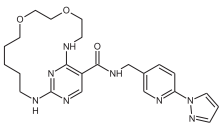	-	-	14000	4.854
67	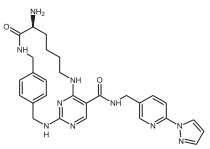	-	-	40	7.398
68	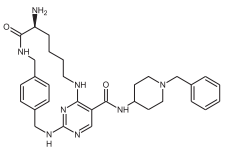	-	-	21	7.678

*Test set compounds

Results and discussion

Activity vs ring size

The dataset comprises macrocyclic compounds with various ring sizes ranging from 14 to 20-members. Since previous reports mentioned about ring size effects over biological activity, we tried to see the ring size effects. As shown in Fig. 1, there seemed no correlation between ring size (*x*-axis) and biological activity (*y*-axis). To further investigate the factors affecting biological activity, we did docking study.

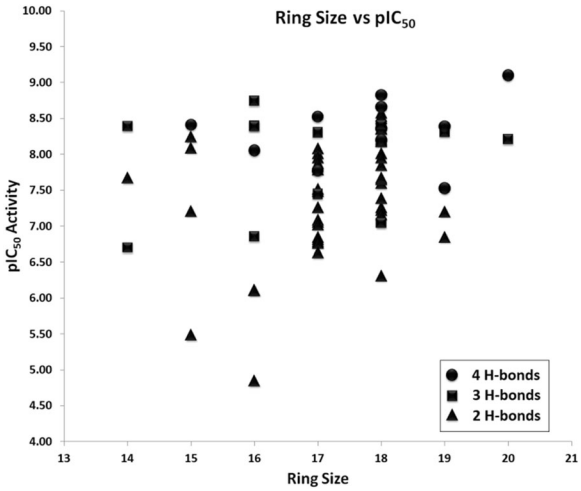

Fig. 1 The scatter plot of macrocyclic ring size vs. pIC_{50} activity values. Circle indicates compounds having four H-bonds; square indicates compounds having three H-bonds and triangle indicates compounds having two H-bonds

Molecular docking and pose optimization using molecular dynamics

In many cases of cyclic inhibitors, docking approaches have been particularly difficult. Most of the docking programs do not support flexibility of the cyclic inhibitors during docking. Hence, pose selection from docked structures was performed to provide flexibility to macrocyclic rings and to get more reliable binding poses for the 3D-QSAR study. MD was used for pose selection of macrocyclic compounds inside the receptor. The MD for each docked compound was carried out for 100 ps with a time step of 1 fs with the abovementioned parameters using dynamics module in Sybyl-X 2.1. The conformers were saved every 5 ps which generated a total of 20 conformers for each compound. The obtained conformers were plotted as scatter plot for each compound based on their energy. From the conformers generated for each compound, one conformation was selected on the basis of the lowest energy and the presence of two signature H-bond interactions with the important hinge region residues Pro672 and Met674. Final conformers selected were used for the alignment of dataset compounds in the 3D-QSAR study. The selected docked structures from MD simulations were used for subsequent 3D-QSAR studies.

Since diverse rings would bind differently to the same receptor, all the compounds were docked. Table 2 shows the docking analyses of all dataset compounds. First, we chose 100 poses for each docked compound. Among them, the best binding pose was selected on the basis of docking score and the key hydrogen bonding for each compound. In Fig. 2a, the binding pose of the most active compound in MerTK is shown. For this cyclic inhibitor, there are four H-bonds with residues at the active site.

The H of **NH** (bold **NH** in Fig. 3) that is adjacent to pyrimidine ring forms H-bond with the hinge region residue Pro672. Similarly, the N (bold **N** in Fig. 3) of pyrimidine ring forms H-bond with the hinge region residue Met674. X-ray crystal structures conducted by McIver et al. (2017) also have two H-bonds at this hinge region. This is consistent with the previous reports that these H-bonds are essential (Balupuri et al. 2015, 2016). These 2 key interactions were found in all the docked compounds having different ring sizes. In addition, hydrogen atoms of the amino group of the macrocyclic ring forms H-bond interactions with the active site residues Arg727 and Asn728. Hydrogen bonding was assigned with PyMOL program with default parameters. From the docking results, the chiral compounds having S configuration in the pyrimidine ring seem to be crucial to form H-bond interactions with the active site residues Arg727 and Asn728. These docked poses explain why group I and III compounds have chiral carbon of S configuration. If the chiral compounds have R configuration, these hydrogen-bonding interactions would not be possible.

Hydrophobic interactions of the most active compound with MerTK were also identified. We have used python script to color receptor according to the Eisenberg hydrophobicity scale (Eisenberg et al. 1984) in PyMOL (Fig. 2b). This gives coloring from red for the most hydrophobic to white for the least hydrophobic. Active site residues that reside in the hydrophobic region (highlighted as sticks in the Fig. 2b) seem to form hydrophobic interactions with the most active compound. Hydrophobic interactions of phenyl ring at the R^1 position with residues Gly677 and Tyr685 and pyrimidine ring with residues Phe673 and Met730 were observed. In addition, the macrocyclic ring was docked into the deep hydrophobic pocket of MerTK, which was lined with residues Val601 and Leu671.

From the overall docking results we could speculate that active site residues Pro672, Met674, Arg727, Asn728, Val601, and Leu671 are important for the binding of the macrocyclic ring inside the binding pocket of MerTK. The

Table 2 Hydrogen bond interactions between macrocyclic pyrimidine derivatives and MerTK (Docking analyses of the dataset compounds)

Compound	Ring size	pIC_{50}	No. of H-bonds	Hydrogen bond residues			
				HB1	HB2	HB3	HB4
Cpd01	15	8.409	4	PRO672	MET674	ARG727	ASN728
Cpd02	17	7.770	4	PRO672	MET674	ARG727	ASN728
Cpd03	19	7.523	4	PRO672	MET674	ARG727	ASN728
Cpd04	16	8.051	4	PRO672	MET674	ARG727	ASN728
Cpd05	18	8.658	4	PRO672	MET674	ARG727	ASN728
Cpd06	20	9.097	4	PRO672	MET674	ARG727	ASN728
Cpd43	19	8.387	4	PRO672	MET674	ARG727	ASN728
Cpd13	17	8.523	4	PRO672	MET674	ASP741	ASN728
Cpd53	18	8.824	4	PRO672	MET674	ARG727	ASN728
Cpd42	18	8.357	4	PRO672	MET674	ARG727	ASN728
Cpd45	18	8.194	4	PRO672	MET674	ARG727	ASN728
Cpd07	14	8.387	3	PRO672	MET674	ASP741	–
Cpd09	16	8.745	3	PRO672	MET674	ASP741	–
Cpd41	17	7.444	3	PRO672	MET674	ASN728	–
Cpd37	18	7.041	3	PRO672	MET674	ARG727	–
Cpd18	19	8.310	3	PRO672	MET674	ASN728	–
Cpd40	16	6.854	3	PRO672	MET674	ASN728	–
Cpd60	18	8.409	3	PRO672	MET674	ASN728	–
Cpd44	20	8.208	3	PRO672	MET674	ASN728	–
Cpd16	17	8.301	3	PRO672	MET674	ASN728	–
Cpd34	14	6.699	3	PRO672	MET674	ASP741	–
Cpd15	16	8.387	3	PRO672	MET674	ASP741	–
Cpd12	16	8.398	2	PRO672	MET674	–	–
Cpd38	19	7.208	2	PRO672	MET674	–	–
Cpd08	15	8.252	2	PRO672	MET674	–	–
Cpd10	17	8.018	2	PRO672	MET674	–	–
Cpd11	15	8.097	2	PRO672	MET674	–	–
Cpd14	18	8.585	2	PRO672	MET674	–	–
Cpd17	18	8.509	2	PRO672	MET674	–	–
Cpd19	17	6.854	2	PRO672	MET674	–	–
Cpd20	17	6.824	2	PRO672	MET674	–	–
Cpd21	17	7.066	2	PRO672	MET674	–	–
Cpd22	17	6.796	2	PRO672	MET674	–	–
Cpd23	17	6.770	2	PRO672	MET674	–	–
Cpd24	17	7.796	2	PRO672	MET674	–	–
Cpd25	17	8.092	2	PRO672	MET674	–	–
Cpd26	17	7.959	2	PRO672	MET674	–	–
Cpd27	17	7.523	2	PRO672	MET674	–	–
Cpd28	17	7.495	2	PRO672	MET674	–	–
Cpd29	17	7.268	2	PRO672	MET674	–	–
Cpd30	17	7.886	2	PRO672	MET674	–	–
Cpd31	17	7.097	2	PRO672	MET674	–	–
Cpd32	17	7.027	2	PRO672	MET674	–	–
Cpd33	15	7.215	2	PRO672	MET674	–	–
Cpd35	16	6.119	2	PRO672	MET674	–	–
Cpd36	17	6.638	2	PRO672	MET674	–	–

Table 2 (continued)

Compound	Ring size	pIC_{50}	No. of H-bonds	Hydrogen bond residues			
				HB1	HB2	HB3	HB4
Cpd39	15	5.495	2	PRO672	MET674	–	–
Cpd46	18	7.602	2	PRO672	MET674	–	–
Cpd47	18	8.222	2	PRO672	MET674	–	–
Cpd48	18	8.022	2	PRO672	MET674	–	–
Cpd49	18	8.367	2	PRO672	MET674	–	–
Cpd50	18	8.201	2	PRO672	MET674	–	–
Cpd51	18	8.357	2	PRO672	MET674	–	–
Cpd52	18	7.658	2	PRO672	MET674	–	–
Cpd54	18	8.187	2	PRO672	MET674	–	–
Cpd55	18	7.854	2	PRO672	MET674	–	–
Cpd56	18	8.538	2	PRO672	MET674	–	–
Cpd57	18	7.268	2	PRO672	MET674	–	–
Cpd58	18	7.229	2	PRO672	MET674	–	–
Cpd59	18	7.959	2	PRO672	MET674	–	–
Cpd61	18	7.168	2	PRO672	MET674	–	–
Cpd62	19	6.854	2	PRO672	MET674	–	–
Cpd63	14	7.678	2	PRO672	MET674	–	–
Cpd64	18	6.319	2	PRO672	MET674	–	–
Cpd65	16	6.114	2	PRO672	MET674	–	–
Cpd66	16	4.854	2	PRO672	MET674	–	–
Cpd67	18	7.398	2	PRO672	MET674	–	–
Cpd68	18	7.678	2	PRO672	MET674	–	–

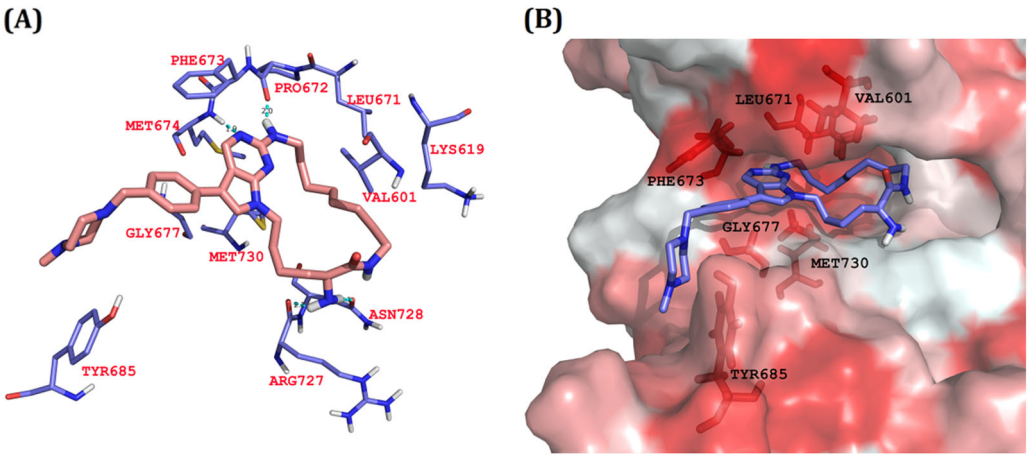

Fig. 2 **a** The docked conformation of the compound 06 (shown in stick model) inside the binding pocket of MerTK Cyan dotted lines represents H-bonds formed between residues and compound 06. H-bond distances are labeled in angstrom. **b** The most active compound (shown in stick model) inside the hydrophobic pocket of MerTK. The red-colored region represents the most hydrophobic surface and white color represents the less hydrophobic surface of the protein

docked conformations of all these compounds were selected based on the presence of the two key H-bond interactions with hinge region residues Pro672 and Met674 similar to that of the most active compound.

Figure 1 shows the scatter plot of macrocyclic ring size versus pIC_{50} activity values. This shows that the various ring-sized compounds possess various inhibitory activities so no significant effect of the ring size over the potency was

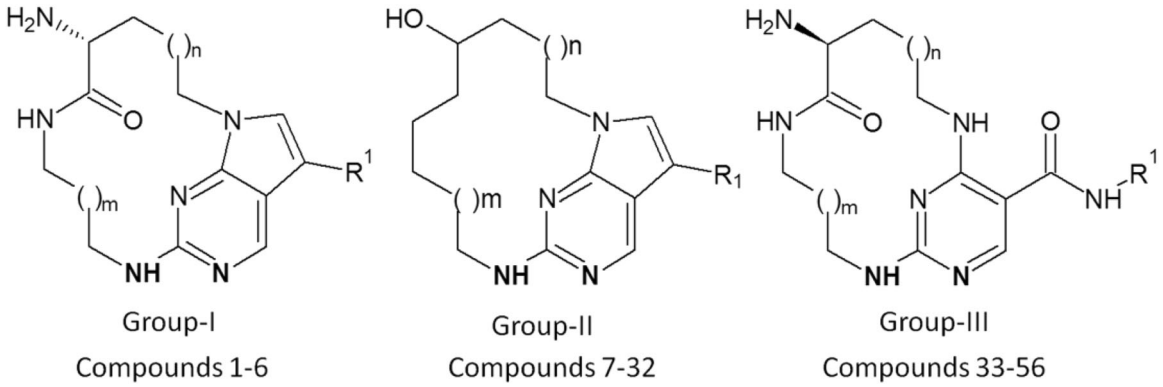

Fig. 3 Dataset compounds (Group I, Group II, and Group III). Dataset compounds were categorized into Group I, Group II, and Group III depending on the amino group having S configuration in the pyrimidine ring and compounds having hydroxyl group in the pyrimidine ring

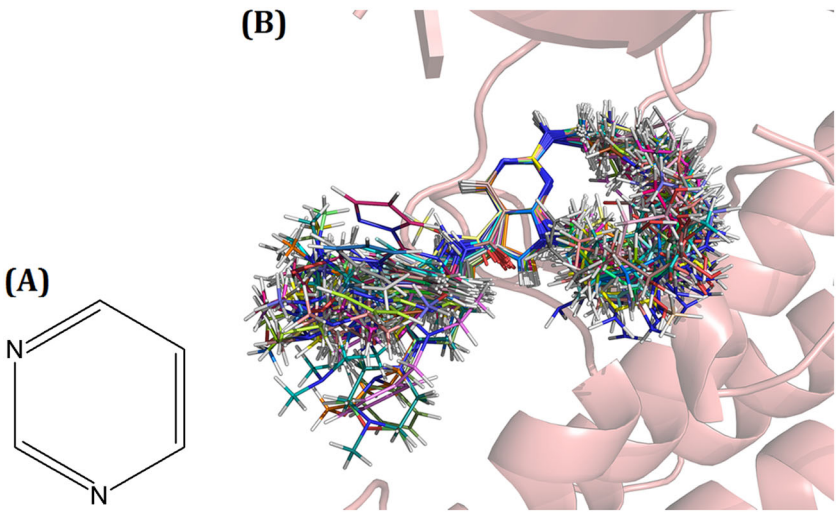

Fig. 4 **a** Common substructure of the dataset. **b** Alignment of the dataset compounds inside the active site of MerTK

observed. However, from our docking analysis it was observed that the compounds with higher activity have more hydrogen-bonding interactions whereas, compounds with lower activity values showed less hydrogen-bonding interactions with the protein. From which it is quite clear that the H-bond formation may have influence on the activity of the compounds rather than the ring-size effect.

CoMFA and CoMSIA

Receptor-based 3D-QSAR models were developed for the series of macrocyclic pyrimidines as potent MerTK inhibitors. Conformers obtained from the pose selection for various ring size compounds were used for the 3D-QSAR study. All the compounds were aligned with the template molecule (most active compound) using the common substructure. The common substructure is shown in Fig. 4a and the alignment of the dataset is shown in Fig. 4b. Choice of appropriate partial charges is crucial to obtain reasonable 3D-QSAR models. Thus, different charge schemes such as Gasteiger–Hückel, Hückel, Gasteiger–Marsili, Del-Re, Pullman, MMFF94, and AM1-BCC were applied.

The dataset was divided into a test set of 22 compounds and a training set of 46 compounds to develop 3D-QSAR models for the external test set. CoMFA models with steric and electrostatic field (S + E) contributions were obtained. Among the different charge schemes used, MMFF94 produced statistically reasonable CoMFA model (S + E) in terms of several statistical parameters ($q^2 = 0.702$, ONC = 5, and $r^2 = 0.979$). Then we developed CoMFA models for electrostatic parameter alone (E only) to minimize the interaction between these parameters. The CoMFA models (E only) is shown in Table 3. MMFF94 produced statistically reasonable model ($q^2 = 0.600$, ONC = 6, and $r^2 = 0.943$). We compared both CoMFA models and found that model with S + E is statistically better than the model with E only. The contour maps obtained from two models (S + E and E only) were

Table 3 Statistical summary of the developed CoMFA models for electrostatic descriptor with different charge schemes

Parameter		Gasteiger–Huckel	Gasteiger–Marsili	MMFF94	Del-Re	Huckel	Pullman	AM1-BCC
E	q^2	0.297	0.315	**0.600**	0.282	0.274	0.379	0.328
	ONC	1	1	**6**	1	2	6	3
	SEP	0.758	0.748	**0.607**	0.766	0.779	0.756	0.671
	r^2	0.792	0.849	**0.943**	0.858	0.651	0.958	0.890
	SEE	0.422	0.359	**0.134**	0.349	0.553	0.197	0.341
	F value	53.409	78.748	**328.045**	84.531	19.149	147.995	86.305

E electrostatic descriptor, q^2 squared cross-validated correlation coefficient, *ONC* optimal number of components, *SEP* standard error of prediction, r^2 squared correlation coefficient, *SEE* standard error of estimation, *F value* F-test value (These models were developed after dividing dataset into trainingset of 46 compounds and test set of 22 compounds. The MMFF94 charge scheme (denoted in bold font) has produced statistically reasonable CoMFAmodel, so it was selected for further studies.)

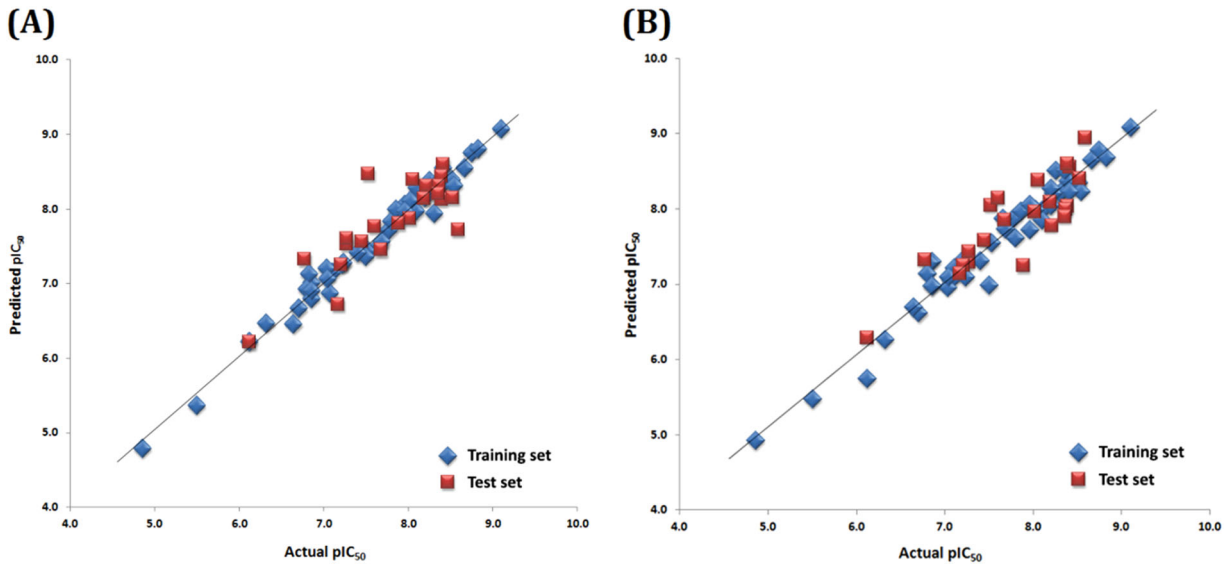

Fig. 5 **a** Scatter plot for the selected CoMFA model. **b** Scatter plot for the selected CoMSIA model. The plot shows the actual pIC_{50} versus predicted pIC_{50} activity of the dataset for training and test sets. The training set compounds are represented as diamonds in blue color; the test set compounds are represented as squares in red color

quite similar. CoMFA model obtained only with electrostatic parameters could explain clearly about the hydrogen bonding. Therefore we have selected this model to validate the notion that hydrogen-bonding interactions could be crucial for the activity variation. The r^2_{pred} value of 0.724 suggests that the model is statistically stable (Pratim Roy et al. 2009). The scatter plot and contour maps is depicted in Figs. 5 and 6, respectively. The CoMFA (E only) contour map results are consistent with our docking analysis which is discussed in detail in the contour map analysis section.

Different combinations of steric (S), electrostatic (E), hydrophobic (H), H-bond acceptor (A), and H-bond donor (D) fields were used to generate the CoMSIA models. Among the charge schemes studied, MMFF94 was used as a partial charge to generate the CoMSIA models by using the similar training set and test set as used in CoMFA. The detailed statistical values for the generated CoMSIA models are depicted in Table S1 of the supplementary material. Among the probable combinations, the optimal CoMSIA model generated using electrostatic and H-bond donor parameters (ED) gave relatively better statistical results ($q^2 = 0.563$, ONC = 5, and $r^2 = 0.927$), therefore selected as the final model. The r^2_{pred} value of 0.672 indicates that the model is statistically reasonable (Pratim Roy et al. 2009). The selected CoMFA (E only) and CoMSIA (ED) models helped us to confirm the hydrogen-bonding interactions observed in docking analysis. It is observed that H-bond interactions with the active site residues Arg727 and Asn728 are important along with the H-bond interactions with 2 key residues Pro672 and Met674 for the inhibition of MerTK.

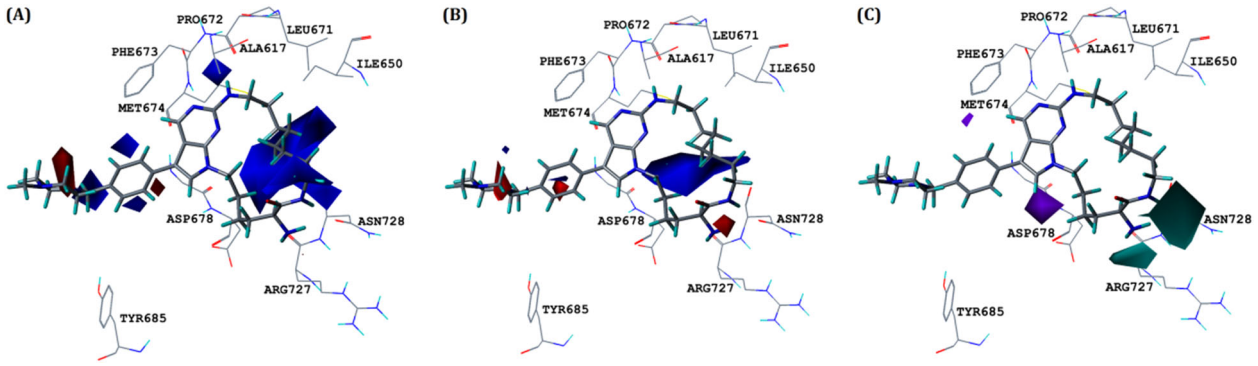

Fig. 6 Contour maps for the selected CoMFA and CoMSIA models. **a** CoMFA electrostatic contour map. **b** CoMSIA electrostatic contour map. **c** CoMSIA H-bond donor contour map. Blue contours favor electropositive substitutions while red contours favor electronegative substitutions. The Cyan contours indicate the favorable region for H-bond donor substitution whereas the purple contours indicate the unfavorable region for H-bond donor substitutions

Table 4 Statistical values of the selected CoMFA and CoMSIA models

Parameters	CoMFA (E only)	CoMSIA (ED)
q^2	0.600	0.563
ONC	6	5
SEP	0.607	0.627
r^2	0.943	0.927
SEE	0.134	0.200
F value	328.045	171.086
BS-r^2	0.987	0.981
BS-SD	0.005	0.010
Q^2	0.413	0.554
r^2_{pred}	0.724	0.672
rm^2	0.593	0.549
Delta rm^2	0.130	0.064
CCC	0.836	0.815

E electrostatic, *D* hydrogen bond donor, q^2 cross-validated correlation coefficient, *ONC* optimal number of components, *SEP* standard error of prediction, r^2 non-validated correlation coefficient, *SEE* standard error of estimation, *F value* F-test value, *BS-*r^2 bootstrapping r^2 mean, *BS-SD* bootstrapping standard deviation, Q^2 progressive scrambling, r^2_{pred} predictive r^2, rm^2 average rm^2 for the dataset, *Delta* rm^2 delta rm^2 for the dataset, *CCC* concordance correlation coefficient

Both the CoMFA and CoMSIA models were validated using bootstrapping, progressive scrambling (Cramer et al. 1988a), rm^2 metric calculation and CCC. The CCC value was found to be significant as per the criteria given by Gramatica et al. (Chirico and Gramatica 2012). The detailed statistical values of the selected CoMFA and CoMSIA models are represented in Table 4. These values suggested that the developed models were statistically reasonable. Table 5 shows the actual and predicted activity values for the final CoMFA and CoMSIA models. The scatter plot and contour maps were depicted in Figs. 5 and 6, respectively.

Contour map analysis

The standard parameters for 3D-QSAR models were used to generate the 3D contour maps that illustrate the change in inhibitory activity according to the changes in physicochemical properties of the substituents. The contour maps for the final CoMFA and CoMSIA models are shown in Fig. 6. The most potent compound of the dataset is shown superimposed with CoMFA and CoMSIA contour maps inside the receptor. Here, we discuss CoMFA model generated only with the electrostatic parameter.

The CoMFA electrostatic contour map is represented in Fig. 6a. The blue contours illustrate the regions where electropositive substitutions increase the activity while red contours illustrate the regions where electronegative substitutions increase the activity. Blue contours are observed at different positions in the macrocyclic ring which suggests that electropositive substitution at these positions increase the activity. The blue contour that is present at **NH** group near pyrimidine ring suggests that electropositive substituent at this position could interact with the Pro672. This can be justified by our docking results in which hydrogen atom from **NH** group forms a H-bond with the oxygen atom of Pro672. This could be the reason for highly active compounds **17, 13, 56, 14, 5, 9**, **53, and 6** (the highest active compound), which have electropositive substitutions at this region. Moreover, the presence of blue contours near phenyl ring of R^1 position signifies the region that is favorable for electropositive substitutions. In contrast, red contours are observed near the piperazine ring at R^1 position and near the phenyl ring. This could be the reason for the moderate activity of the compounds **58** and **59** which possess electronegative substituent at these positions.

Since electrostatic contour map in CoMFA (Fig. 6a) is almost similar to the CoMSIA electrostatic contour (Fig. 6b), only the H-bond donor contour map of CoMSIA is discussed below. The H-bond donor contour map from

Table 5 Actual pIC_{50} and predicted pIC_{50} values with their residual values of selected CoMFA and CoMSIA models

Compound	Actual pIC_{50}	CoMFA (E only)		CoMSIA (ED)	
		Predicted pIC_{50}	Residual	Predicted pIC_{50}	Residual
1	8.555	8.507	−0.098	8.555	−0.146
2	7.880	7.718	0.052	7.880	−0.110
3	8.450	8.484	−0.961	8.450	−0.927
4	8.391	8.207	−0.156	8.391	−0.340
5	8.658	8.556	0.102	8.656	0.002
6	9.097	9.075	0.022	9.090	0.007
7	8.387	8.137	0.250	8.603	−0.216
8	8.252	8.376	−0.124	8.519	−0.267
9	8.745	8.756	−0.011	8.787	−0.042
10	8.018	7.879	0.139	7.965	0.053
11	8.097	8.283	−0.186	7.989	0.108
12	8.398	8.361	0.037	8.290	0.108
13	8.523	8.459	0.064	8.409	0.114
14	8.585	7.734	0.851	8.948	−0.363
15	8.387	8.330	0.057	8.374	0.013
16	8.301	7.943	0.358	8.216	0.085
17	8.509	8.393	0.116	8.352	0.157
18	8.310	8.318	−0.008	8.226	0.084
19	6.854	7.019	−0.165	7.310	−0.456
20	6.824	7.130	−0.306	7.295	−0.471
21	7.066	6.878	0.188	7.058	0.008
22	6.796	6.933	−0.137	7.151	−0.355
23	6.770	7.334	−0.564	7.330	−0.560
24	7.796	7.841	−0.045	7.625	0.171
25	8.092	7.973	0.119	7.860	0.232
26	7.959	8.057	−0.098	7.734	0.225
27	7.523	7.440	0.083	7.553	−0.030
28	7.495	7.370	0.125	6.994	0.501
29	7.268	7.540	−0.272	7.292	−0.024
30	7.886	7.815	0.071	7.149	0.737
31	7.097	7.157	−0.060	7.227	−0.130
32	7.027	7.204	−0.177	6.968	0.059
33	7.215	7.263	−0.048	7.337	−0.122
34	6.699	6.669	0.030	6.630	0.069
35	6.119	6.222	−0.103	6.294	−0.175
36	6.638	6.462	0.176	6.708	−0.070
37	7.041	7.065	−0.024	7.099	−0.058
38	7.208	7.262	−0.054	7.256	−0.048
39	5.495	5.370	0.125	5.480	0.015
40	6.854	6.800	0.054	6.989	−0.135
41	7.444	7.574	−0.130	7.589	−0.145
42	8.357	8.356	0.001	8.523	−0.166
43	8.387	8.442	−0.055	8.036	0.351
44	8.208	8.317	−0.109	7.785	0.423
45	8.194	8.156	0.038	8.056	0.138
46	7.602	7.776	−0.174	8.148	−0.546
47	8.222	8.231	−0.009	8.220	0.002
48	8.022	8.113	−0.091	7.996	0.026
49	8.367	8.315	0.052	7.995	0.372
50	8.201	8.256	−0.055	8.278	−0.077
51	8.357	8.214	0.143	7.906	0.451
52	7.658	7.516	0.142	7.881	−0.223
53	8.824	8.811	0.013	8.690	0.134
54	8.187	8.152	0.035	8.090	0.097
55	7.854	7.992	−0.138	7.983	−0.129
56	8.538	8.320	0.218	8.241	0.297
57	7.268	7.615	−0.347	7.433	−0.165
58	7.229	7.281	–0.052	7.102	0.127
59	7.959	7.972	−0.013	8.069	−0.110
60	8.409	8.549	−0.140	8.233	0.176
61	7.168	6.732	0.436	7.144	0.024
62	6.854	6.910	−0.056	6.987	−0.133
63	7.678	7.461	0.217	7.857	−0.179
64	6.319	6.467	−0.148	6.269	0.050
65	6.114	6.226	−0.113	5.756	0.358
66	4.854	4.792	0.062	4.934	−0.080
67	7.398	7.417	−0.019	7.319	0.079
68	7.678	7.565	0.113	7.737	−0.059

CoMSIA is shown in Fig. 6c. The cyan contours indicate the favorable regions for H-bond donor groups, while the purple contours indicate the unfavorable regions for H-bond donor groups. Cyan contours on both sides of the amino group of macrocyclic ring suggest that the presence of H-bond donor group at these positions could increase the activity. This could be due to the fact that the H-bond donor substitutions at these regions could interact with the oxygen atoms of residues Arg727 and Asn728. These interactions are observed in our docking analyses. This can also be explained by the moderate to the high activity of compounds **17, 13, 56, 14, 5, 9**, **53, and 6** (the highest active compound) which possess H-bond donor group in this region. On the contrary, the purple contours around the pyrimidine ring are unfavorable for the H-bond donor groups and could cause decrease in the efficacy. Overall contour map analysis supports the notion that the H-bond formation has influence on the activity of the compounds rather than the ring-size effect.

Conclusion

In this study, we have performed molecular docking of the macrocyclic pyrimidines followed by their pose selection and 3D-QSAR to understand the factors involving a series of macrocyclic inhibitors against MerTK. Molecular docking of these different sized compounds (14–20-membered rings) was carried out to check their binding affinity to MerTK. Docking studies revealed the interactions with crucial active site residues; i.e., in addition to two signature H-bond interactions (Pro672 and Met674), the two H-bond interactions with Arg727 and Asn728 were found essential. Furthermore, active site residues Val601, Leu671, Phe673, Gly677, Tyr685, and Met730 were observed which form hydrophobic pocket. Though the ring size effect was not observed, our results support the importance of hydrogen bonding. Moreover, the importance of number of hydrogen bonding was confirmed statistically by receptor-based CoMFA and CoMSIA models and further visualized by their contour maps. These models were validated by various statistical parameters such as bootstrapping, progressive scrambling, an external test set validation, rm^2 metric calculations and CCC. The analysis of overall contour maps suggested that the electropositive substitution near the pyrimidine ring and at R^1 position are favored to increase the activity. Likewise, electropositive and hydrogen-bonding donor groups are favorable in the macrocyclic ring.

Overall, our results provide the importance of hydrogen-bonding interactions for this receptor along with suggested critical residues, which could be useful for more potent MerTK inhibitor design. In addition, this work suggests the importance of hydrogen bonding for macrocyclic compounds as inhibitors, at least for the series of the compounds used in this study. However, if the dataset is different, this conclusion may not be applicable. To understand macrocyclic effects more clearly in drug discovery, further detailed studies should be desirable over this issue.

Acknowledgements This work was supported by the National Research Foundation of Korea grant (MRC, 2015-009070) and Basic Science Research Program through the National Research Foundation of Korea (NRF) funded by the Ministry of Education, Science and Technology (NRF-2016RID1AIB01007060).

Compliance with ethical standards

Conflict of interest The authors declare that they have no conflict of interest.

References

Balupuri A, Balasubramanian PK, Cho SJ (2015) Molecular modeling study on Mer kinase inhibitors using 3D-QSAR and docking approaches. Med Chem Res 24:3730–3742

Balupuri A, Balasubramanian PK, Cho SJ (2016) Determination of structural requirements of Mer kinase inhibitors and binding interaction analysis using in silico approaches. Med Chem Res 25:3021–3029

Berthod H, Giessner-Prettre C, Pullman A (1967) Sur les rôles respectifs des électrons σ et π dans les propriétés des dérivés halogénés des molécules conjuguées. application à l'étude de l'uracile et du fluorouracile. Theor Chim Acta 8:212–222

Bridger GJ, Skerlj RT, Thornton D, Padmanabhan S, Martellucci SA, Henson GW, Abrams MJ, Yamamoto N, Vreese KD, Pauwels R, De Clercq E (1995) Synthesis and structure-activity relationships of phenylenebis (methylene)-linked bis-tetraazamacrocycles that inhibit HIV replication. Effects of macrocyclic ring size and substituents on the aromatic linker. J Med Chem 38:366–378

Chirico N, Gramatica P (2012) Real external predictivity of QSAR models. Part 2. New intercomparable thresholds for different validation criteria and the need for scatter plot inspection. J Chem Inf Model 52:2044–2058

Clark M, Cramer RD, Van Opdenbosch N (1989) Validation of the general purpose Tripos 5.2 force field. J Comput Chem 10:982–1012

Cramer RD (1993) Partial least squares (PLS): its strengths and limitations. Perspect Drug Discov Des 1:269–278

Cramer RD, Bunce JD, Patterson DE, Frank IE (1988a) Cross-validation, bootstrapping, and partial least squares compared with multiple regression in conventional QSAR studies. Mol Inform 7:18–25

Cramer RD, Patterson DE, Bunce JD (1988b) Comparative molecular field analysis (CoMFA). 1. Effect of shape on binding of steroids to carrier proteins. J Am Chem Soc 110:5959–5967

Craven RJ, Xu L, Weiner TM, Fridell YW, Dent GA, Srivastava S, Varnum B, Liu ET, Cance WG (1995) Receptor tyrosine kinases expressed in metastatic colon cancer. Int J Cancer 60:791–797

Cummings CT, Deryckere D, Earp HS, Graham DK (2013) Molecular pathways: MERTK signaling in cancer. Clin Cancer Res 19:5275–5280

Del Re G (1958) 812. A simple MO–LCAO method for the calculation of charge distributions in saturated organic molecules. J Chem Soc (Resumed) 4031–4040. https://doi.org/10.1039/JR9580004031

Driggers EM, Hale SP, Lee J, Terrett NK (2008) The exploration of macrocycles for drug discovery—an underexploited structural class. Nat Rev Drug Discov 7:608

Eisenberg D, Schwarz E, Komaromy M, Wall R (1984) Analysis of membrane and surface protein sequences with the hydrophobic moment plot. J Mol Biol 179:125–142

Evans AL, Blackburn JW, Taruc K, Kipp A, Dirk BS, Hunt NR, Barr SD, Dikeakos JD, Heit B (2017) Antagonistic coevolution of MER tyrosine kinase expression and function. Mol Biol Evol 34:1613–1628

Gadhe CG, Kothandan G, Cho SJ (2012) Large variation in electrostatic contours upon addition of steric parameters and the effect of charge calculation schemes in CoMFA on mutagenicity of MX analogues. Mol Simul 38:861–871

Gasteiger J, Marsili M (1980) Iterative partial equalization of orbital electronegativity—a rapid access to atomic charges. Tetrahedron 36:3219–3228

Giordanetto F, Kihlberg J (2013) Macrocyclic drugs and clinical candidates: what can medicinal chemists learn from their properties? J Med Chem 57:278–295

Gradillas A, and Perez-Castells J (2010) Synthesis of Natural Products Containing Macrocycles by Alkene Ring-Closing Metathesis. Metathesis in Natural Product Synthesis: Strategies, Substrates and Catalysts 149–182. https://doi.org/10.1002/9783527629626.ch5

Graham DK, Dawson TL, Mullaney DL, Snodgrass HR, Earp HS (1994) Cloning and mRNA expression analysis of a novel human protooncogene, c-mer. Cell growth & differentiation: the molecular biology journal of the American Association for. Cancer Res 5:647–657

Halgren TA (1999) MMFF VI. MMFF94s option for energy minimization studies. J Comput Chem 20:720–729

Hamzah N, and Tjahjono DA (2016) Quantitative Structure-Activity Relationship Study, Compound Development, Pharmacophore Feature, and Molecular Docking of Pyrazolo-[3, 4-d]-Pyrimidine Derivatives as Mer Tyrosine Kinase Inhibitor. Int J Chemtech Res 9:323–337

Hawkins PC (2017) Conformation generation: the state of the art. J Chem Inf Model 57:1747–1756

Hojjat-Farsangi M (2014) Small-molecule inhibitors of the receptor tyrosine kinases: promising tools for targeted cancer therapies. Int J Mol Sci 15:13768–13801

Holland SJ, Pan A, Franci C, Hu Y, Chang B, Li W, Duan M, Torneros A, Yu J, Heckrodt TJ (2010) R428, a selective small molecule inhibitor of Axl kinase, blocks tumor spread and prolongs survival in models of metastatic breast cancer. Cancer Res 70:1544–1554

Holland SJ, Powell MJ, Franci C, Chan EW, Friera AM, Atchison RE, Mclaughlin J, Swift SE, Pali ES, Yam G (2005) Multiple roles for the receptor tyrosine kinase axl in tumor formation. Cancer Res 65:9294–9303

Huey R, Morris GM, Olson AJ, Goodsell DS (2007) A semiempirical free energy force field with charge-based desolvation. J Comput Chem 28:1145–1152

Jakalian A, Jack DB, Bayly CI (2002) Fast, efficient generation of high-quality atomic charges. AM1-BCC model: II. Parameterization and validation. J Comput Chem 23:1623–1641

Kamath S, Buolamwini JK (2003) Receptor-guided alignment-based comparative 3D-QSAR studies of benzylidene malonitrile tyrphostins as EGFR and HER-2 kinase inhibitors. J Med Chem 46:4657–4668

Klebe G, Abraham U, Mietzner T (1994) Molecular similarity indices in a comparative analysis (CoMSIA) of drug molecules to correlate and predict their biological activity. J Med Chem 37:4130–4146

Knubel KH, Pernu BM, Sufit A, Nelson S, Pierce AM, Keating AK (2014) MerTK inhibition is a novel therapeutic approach for glioblastoma multiforme. Oncotarget 5:1338

Lemke G, Rothlin CV (2008) Immunobiology of the TAM receptors. Nat Rev Immunol 8:327

Li Y-P, Weng X, Ning F-X, Ou J-B, Hou J-Q, Luo H-B, Li D, Huang Z-S, Huang S-L, Gu L-Q (2013) 3D-QSAR studies of azaoxoisoaporphine, oxoaporphine, and oxoisoaporphine derivatives as anti-AChE and anti-AD agents by the CoMFA method. J Mol Graph Model 41:61–67

Liang F, Wan S, Li Z, Xiong X, Yang L, Zhou X, Wu C (2006) Medical applications of macrocyclic polyamines. Curr Med Chem 13:711–727

Linger RM, Keating AK, Earp HS, Graham DK (2008) TAM receptor tyrosine kinases: biologic functions, signaling, and potential therapeutic targeting in human cancer. Adv cancer Res 100:35–83

Madhavan T, Gadhe CG, Kothandan G, Lee K, Cho SJ (2012) Various atomic charge calculation schemes of CoMFA on HIF-1 inhibitors of moracin analogs. Int J Quantum Chem 112:995–1005

Madsen CM, Clausen MH (2011) Biologically active macrocyclic compounds–from natural products to diversity-oriented synthesis. Eur J Org Chem 2011:3107–3115

Mallinson J, Collins I (2012) Macrocycles in new drug discovery. Future Med Chem 4:1409–1438

Marsault E, Peterson ML (2011) Macrocycles are great cycles: applications, opportunities, and challenges of synthetic macrocycles in drug discovery. J Med Chem 54:1961–2004

Marsault E, Peterson ML (2017) Practical Medicinal Chemistry with Macrocycles: Design, Synthesis, and Case Studies, John Wiley & Sons. Place. ISBN: 978-1-119-09256-8

Mciver AL, Zhang W, Liu Q, Jiang X, Stashko MA, Nichols J, Miley MJ, Norris-Drouin J, Machius M, Deryckere D (2017) Discovery of macrocyclic pyrimidines as MerTK-specific inhibitors. ChemMedChem 12:207–213

Neubauer A, Fiebeler A, Graham DK, O'bryan JP, Schmidt CA, Barckow P, Serke S, Siegert W, Snodgrass HR, Huhn D (1994) Expression of axl, a transforming receptor tyrosine kinase, in normal and malignant hematopoiesis. Blood 84:1931–1941

Nguyen K-QN, Tsou W-I, Calarese DA, Kimani SG, Singh S, Hsieh S, Liu Y, Lu B, Wu Y, Garforth SJ (2014) Overexpression of MERTK receptor tyrosine kinase in epithelial cancer cells drives efferocytosis in a gain-of-function capacity. J Biol Chem 289:25737–25749

Pratim Roy P, Paul S, Mitra I, Roy K (2009) On two novel parameters for validation of predictive QSAR models. Molecules 14:1660–1701

Schlegel J, Sambade MJ, Sather S, Moschos SJ, Tan A-C, Winges A, Deryckere D, Carson CC, Trembath DG, Tentler JJ (2013) MERTK receptor tyrosine kinase is a therapeutic target in melanoma. J Clin Investig 123:2257–2267

Wang X, Liu J, Zhang W, Stashko MA, Nichols J, Miley MJ, Norris-Drouin J, Chen Z, Machius M, Deryckere D (2016) Design and synthesis of novel macrocyclic Mer tyrosine kinase inhibitors. ACS Med Chem Lett 7:1044–1049

Watts KS, Dalal P, Tebben AJ, Cheney DL, Shelley JC (2014) Macrocycle conformational sampling with MacroModel. J Chem Inf Model 54:2680–2696

Wessjohann LA, Ruijter E, Garcia-Rivera D, Brandt W (2005) What can a chemist learn from nature's macrocycles?–A brief, conceptual view. Mol Divers 9:171–186

Wold S, Ruhe A, Wold H, Dunn I Wj (1984) The collinearity problem in linear regression. The partial least squares (PLS) approach to generalized inverses. SIAM J Sci Stat Comput 5:735–743

Yu J, Rupasinghe C, Wilson JL, Taylor L, Rahimi N, Mierke D, Polgar P (2015a) Targeting receptor tyrosine kinases and their downstream signaling with cell-penetrating peptides in human pulmonary artery smooth muscle and endothelial cells. Chem Biol Drug Des 85:586–597

Yu Z, Li X, Ge C, Si H, Cui L, Gao H, Duan Y, Zhai H (2015b) 3D-QSAR modeling and molecular docking study on Mer kinase inhibitors of pyridine-substituted pyrimidines. Mol Divers 19:135–147

Zhou S, Zhou L, Cui R, Tian Y, Li X, You R, Zhong L (2016) Pharmacophore-based 3D-QSAR modeling, virtual screening and molecular docking analysis for the detection of MERTK inhibitors with novel scaffold. Comb Chem high throughput Screen 19:73–96